SIMULATION OF SUPERSONIC CATALYTIC GREEN PROPELLANT NOZZLE ROCKET ENGINE

Annibal Hetem

Universidade Federal do ABC - UFABC
annibal.hetem@ufabc.edu.br

Caio Fuzaro Rafael

Universidade Federal do ABC - UFABC
Rua Santa Adélia, 166. Bairro Bangu. Santo André - SP - Brasil . CEP 09.210-170
caio.rafael@aluno.ufabc.edu.br

José Miraglia

Faculdade de Informática e Administração Paulista - FIAP
Av. Lins de Vasconcelos, 1222 e 1264 - São Paulo, SP 01538-001
miragli@terra.com.br

Abstract: *We present simulations of the flow in an engine coupled to a catalytic reaction combustion chamber. The catalytic chamber promotes the dissociation of hydrogen peroxide, whose results react with ethanol. There are also considered propellants details as well as environmental aspects. The pair ethanol / hydrogen peroxide (green propellants) has a higher density than most of the propellants, requires a smaller volume reservoir, decreasing the intrinsic weight of the vehicle. Moreover, hydrogen peroxide and ethanol have lower toxicity than other conventional propellants, still presenting good reason fuel/oxidant. The mixture is storable for long periods of time without the need for cryogenic; being compatible with low-cost construction materials such as aluminum and stainless steel. The low cost is an advantage, since Brazil produces large amounts of ethanol, about 16 million tons per year, and hydrogen peroxide production is about 220,000 tons per year. The numerical simulations of compressible flow passing through a 3D liquid rocket motor convergent-divergent nozzle with a fixed geometry are carried out. Finally, we present results from simulations of 3-D finite volume solver based on the OpenFOAM package. We conclude that the catalytic combustion chamber coupled to the described nozzle can produce enough gas expansion to assure the necessary thrust for a small-medium rocket.*

Keywords: *rocket engine nozzle; CFD simulation; catalytic chamber; ethanol.*

Nomenclature

A:	nozzle area
A_0:	nozzle area at the throat
AEB:	Brazilian Space Agency
C_v:	gas specific heat at constant volume
d_0:	nozzle diameter at the throat
g:	acceleration of gravity
γ:	ratio of specific heats
e:	gas internal energy
ε:	nozzle expansion area ratio
k:	gas thermal conductivity
IAE:	Aeronautics and Space Institute (Brazil)
I_{sp}:	specific impulse
M:	Mach number
$\dot{m}$:	gas mass rate
p:	gas pressure
p_0:	gas pressure at the throat
PCS:	"Programa Cruzeiro do Sul"
r:	nozzle radius
r_e:	nozzle outlet radius
R_x:	desired length ratio to a 15^o conical nozzle
ρ:	gas density
ρ_0:	gas density at the throat
t:	time
T:	gas temperature
T_0:	gas temperature at the throat
V:	total (vector) velocity whose components are u, v and w
V_e:	gas exhaust velocity
VLS:	satellite launch vehicle
x_e:	total nozzle length

1 Introduction

According to the AEB (Brazilian Space Agency) current and future space missions require Brazilian capability to place payloads in the range from 1500 kg to tens of tons. According to Sutton and Biblarz (2001) for this category of launchers it is needed to develop engines that use liquid propellant. Today in Brazil, projects of such

engines have been proposed by IAE (Aeronautics and Space Institute) through the “Programa Cruzeiro do Sul” (PCS). Rockets of different sizes are previewed in this program, like the Alpha VLS, VLS-1's successor. Other models are being planned L5, L15 and L75, which are modular and can be utilized in other projects. An example is the L75, which will be used in the third stage of the VLS Alpha, and the upper stages of launchers Beta, Gamma and Delta all PCS launchers (Torres *et al.* 2009).

Recently, many researchers have endeavored to improve the performance of rocket engines, and these studies used CFD simulations to achieve their goals. A good example is the simulations from Hagemann *et al.* (1998) on altitude-adaptive nozzle concepts. They concluded that flow phenomena observed in numerical simulations during different nozzle operations can help dealing with critical design aspects and operation conditions. Davis *et al.* (2006) studied the flow physics associated with the possibility of thrust augmentation, and their simulations shows that propellant injection downstream of the throat is a viable method for augmenting rocket thrust. In an interesting study on the Ariane V rocket propulsion, Cabrit & Artal (2007) showed that the classical law of the wall for velocity and temperature are not appropriate to represent the numerical results. On the other hand, they demonstrated that chemical equilibrium assumption is shown to be valid in the inert case and a wall function consistent with this assumption is in fair agreement with their results. Balabel and collaborators (2009) demonstrated the numerical accuracy of different turbulent models that can predict the physical properties and physical phenomena of turbulent gas flow in a solid rocket nozzle. In their work, the time-dependent, compressible Navier-Stokes equations with turbulent effects were solved using a 2-D finite volume Navier Stokes solver based on the SIMPLE algorithm. In a study of new injection systems, Pandey (2010) presented some CFD analysis of pressure and temperature for a rocket nozzle with four inlets at Mach 2.1. His results show that when the propellants enter in the combustion chamber in a given geometry its burning is due to high velocity and temperature and then temperature increases rapidly in combustion chamber and convergent part of the nozzle and after that temperature decreases in the exit part of the nozzle. He concludes that four inlet rocket nozzle should have better performance than single inlet and two inlets.

The main piece of software used for the simulations presented in this work were carried out with the OpenFOAM package (that is very well described by Böhm 2011). Some works of other researchers inspired us to test and use this package. For example, Zheng & Sun (2011) accomplished an OpenFOAM simulation of a compressible flow field using a Favre averaged Navier-Stokes control equation with a standard turbulence model. Their convection term and diffusion term were discretized using a second-order accurate total variation diminishing scheme and a second-order central-difference scheme respectively, and then the discretized equations were solved using the SIMPLER (semi-implicit method for pressure-linked equations-revised) method. OpenFOAM was also used by the Bansal team (Bansal *et al.* 2012) to simulate the hypersonic flow and radiation over a Mars reentry vehicle. The simulations highlighted the effects of radiative cooling on flow fields and wall fluxes.

The present work presents an important step in the project of an academic platform developed for rocket engine studies. As a result, it is intended to obtain a complete prototype that should contain all the usual components of such design. The behavior of the engine will be compared with the theory and the like, in order to lead students to an understanding of the processes and methods and also to a critical evaluation of the chosen technologies in different cases. The computations presented in this work were developed at the computational facilities of the Aerospace Engineering course at Federal University of ABC.

In the next section there are presented the first calculations for the design of the nozzle. Then, we present the details of the numerical simulation of the behavior of gases in the nozzle. The simulation results along with some comments finalize this work.

2 Before-nozzle details

In this section it is presented some aspects that lead to the simulation of the gases behavior in the nozzle. First are presented the catalytic combustion chamber concerns, followed by the nozzle design challenges.

2.1 Catalytic combustion chamber

As we intend to adopt the mixture ethanol+hydrogen peroxide as fuel, it is important to discuss its qualities and properties. This mixture, in addition to being easy to handle, does not generate hazardous waste to the environment, are easily accessible, and do not require extreme care in transportation and storage. At normal ambient temperatures, the propellants present themselves in the liquid state already mixed, therefore acting as a mono propellant, what makes the overall rocket project a lot easier. In addition, ethanol belongs to the category of green propellants, and Brazil produces large amounts of ethanol (16 million tons per year) and hydrogen peroxide (220,000 tons per year).

In the proposed design, the combustion chamber is preceded by a catalytic chamber, in which the hydrogen peroxide separation occurs and results subsequently react with ethanol (Fig. 1). For the calculation of the combustion chamber results from the use of Gas Dynamics software Lab. A combustion chamber with 1282.5 cm^3 shall be sufficient for proper burning of the propellant, and that will be necessary to install 24 injectors with 2 mm in diameter. The speed of injection of the propellant must be 19.04 m/s. Upon reaching the nozzle throat, the resulting gases are at T_0=1461 K under a pressure p_0=2,53 MPa (25 atm) (Miraglia *et al.* 2011). These values of pressure and temperature do not reflect actual data, but serve only as a starting point for the simulations presented in this work. In the sequence of this project we are providing studies for simulations of the combustion chamber that will bring us more accurate results on these values.

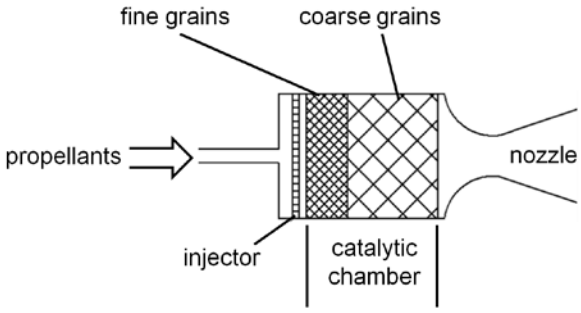

Figure 1. Details of the catalytic chamber and nozzle

2.2 Nozzle profiles

For further interpretation and validation of results, consider the Mach number variation through the nozzle, as given by expression 7.6 from Anderson (1995), derived for a quasi-one-dimensional nozzle flow:

$$\left(\frac{A}{A_0}\right)^2 = \frac{1}{M^2}\left[\frac{2}{\gamma+1}\left(1+\frac{\gamma-1}{2}M^2\right)\right]^{(\gamma+1)/(\gamma-1)} \tag{1}$$

where M, the Mach number, is governed exclusively by the area ratio, A/A_0, and γ, the ratio of specific heats. Eq. (1) permits the implicit calculation of M as a function of x, the position length along the nozzle. From (1) it is possible to obtain

$$\frac{p}{p_0} = \left[1+\frac{\gamma-1}{2}M^2\right]^{-\gamma/(\gamma-1)} \tag{2}$$

$$\frac{\rho}{\rho_0} = \left[1+\frac{\gamma-1}{2}M^2\right]^{-1/(\gamma-1)} \tag{3}$$

$$\frac{T}{T_0} = \left[1+\frac{\gamma-1}{2}M^2\right]^{-1} \tag{4}$$

where p/p_0, ρ/ρ_0 and T/T_0 are the ratios of the pressure, density and temperature at a given point of the nozzle and at the nozzle throat.

The specific nozzle in study in this paper must generate thrust by converting thermal energy of hot combustion gases in kinetic energy. Maximum theoretical thrust is achieved in vacuum conditions when the nozzle area ratio is infinite. In an ideal nozzle, the exit flow is completely parallel to the nozzle axis and possesses uniform pressure and Mach number. By calculating the momentum of the actual nozzle exit flow and comparing it to the parallel, uniform flow condition, the geometric efficiency is determined. By careful shaping of the nozzle wall, relatively high geometric efficiency can be realized (Cornelisse *et al.* 1979).

So, the optimum nozzle contour is a design compromise that results in maximum overall nozzle efficiency. Rao (1958) presents a method for analytically defining this unique contour, and also described in detail by NASA (1976). By shaping the nozzle wall according to their method, a shorter nozzle and an improvement of over one percent in nozzle efficiency can be obtained relative to a 15° cone. We developed a program written in C++

language that applies the Rao method to project a parabolic shaped nozzle. The main entry parameters are throat diameter, d_0, desired length ratio to a 15° conical nozzle, R_x, and the expansion area ratio, ε. Figure 2 presents the main window of this program, with a parabolic shaped nozzle with d_0=5 cm, R_x = 80% and ε = 10. From the combustion chamber interface to the nozzle outlet, the total length is about x_e=19.5 cm, with an outlet radius of about r_e=8 cm.

The resulting shape is recorded to a file in the proper format to be used by the CFD grid-mesh generator. Also provided is an output file for feeding a CNC lathe, in order to build a prototype.

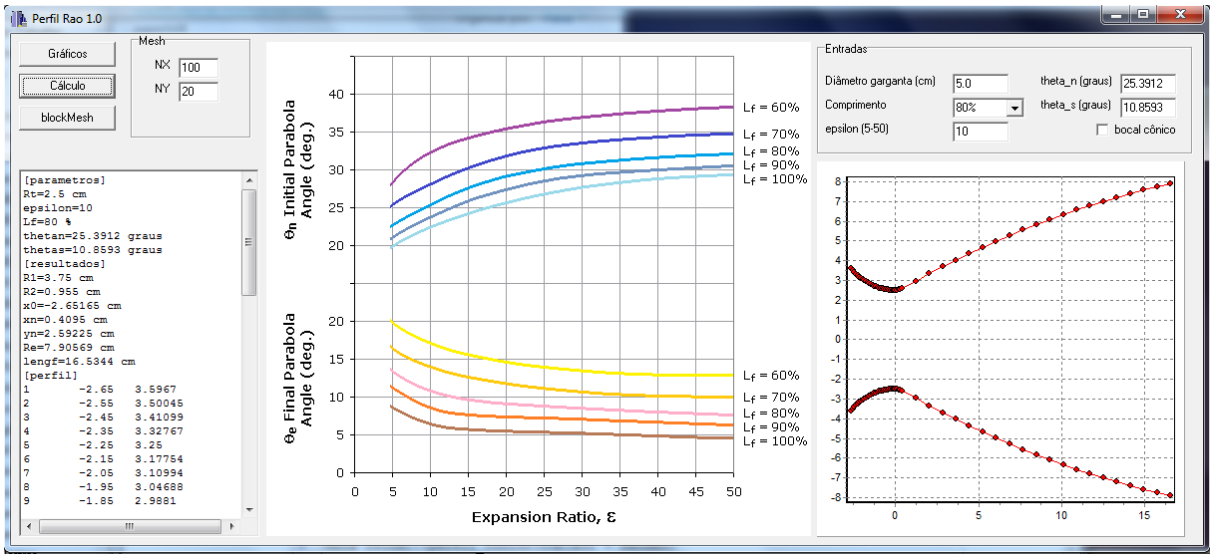

Figure 2. Parabolic profile nozzle designer program main window

3 CFD simulations

This section presents the main aspects of the CFD simulation whose results can be appreciated in section 4. Starting with the equations and conditions, then we present the mesh generation used and finally the PDE solver and visualization techniques.

3.1 Governing equations and conditions

Here we present the governing equation system for the model of the flow inside the nozzle:

$$\frac{\partial \rho}{\partial t} + \nabla \cdot (\rho \mathbf{V}) = 0 \tag{5}$$

$$\frac{\partial (\rho u)}{\partial t} + \nabla \cdot (\rho u \mathbf{V}) = -\frac{\partial p}{\partial x} \tag{6}$$

$$\frac{\partial (\rho v)}{\partial t} + \nabla \cdot (\rho v \mathbf{V}) = -\frac{\partial p}{\partial y} \tag{7}$$

$$\frac{\partial (\rho w)}{\partial t} + \nabla \cdot (\rho w \mathbf{V}) = -\frac{\partial p}{\partial z} \tag{8}$$

$$\frac{\partial \rho e}{\partial t} + \nabla \cdot \rho \mathbf{V} e - \nabla \cdot \left(\frac{k}{C_v} \right) \nabla e = p \nabla \cdot \mathbf{V} \tag{9}$$

$$p = \rho R T \tag{10}$$

where ρ is the mass density; t is time; $\mathbf{V}$ is the velocity vector whose components are u, v and w; x, y, and z are the Cartesian space coordinates; e is the internal energy; k is the thermal conductivity; C_v is specific heat at constant volume; and T is the temperature. Eqs. (5) to (9) are respectively the continuity, momentum (for the three axis) and energy expressions for a coupled system of nonlinear partial equations for a trans-

sonic/supersonic flow of an isentropic, inviscid, compressible flow, and Eq. (10) is a state equation for closing the system, where we consider R=396 m^2/s^2K. For further information, please consult chapter 2 of Anderson (1995) and Böhm (2011).

3.2 Grid-mesh generation

The perfect fluid steady isentropic flow in a converging-diverging nozzle was modeled using a system of two first order partial differential equations in the primary variables. A least square/formulation transforms the first-order system into an equivalent second-order system well adapted to discretization methods and allowing the use Newton's method which yield fast convergence (Bruneau *et al.* 1982).

Assuming cylindrical symmetry in the x direction, the grid was created as a sector of 5^o (1.4%) of the nozzle, with 100 columns along the symmetry axis and 20 layers in the radial direction. Figure 3 presents the final geometry - the mesh actually used in the simulations - generated by the mesh package from OpenFOAM. In the (a) *x-z* view one can see the main features of the adopted geometry. The faces are named according to its role in the simulation: the main fluid goes from the "inlet" to the "outlet" and the nozzle geometry is provided by the "wall" surface, whose shape description is given in Section 2.2. The identification "n-axis" is not of a surface, but of the cylindrical system symmetry axis along the centre of the nozzle. In the (b) *y-z* view one can see the outlet surface face on.

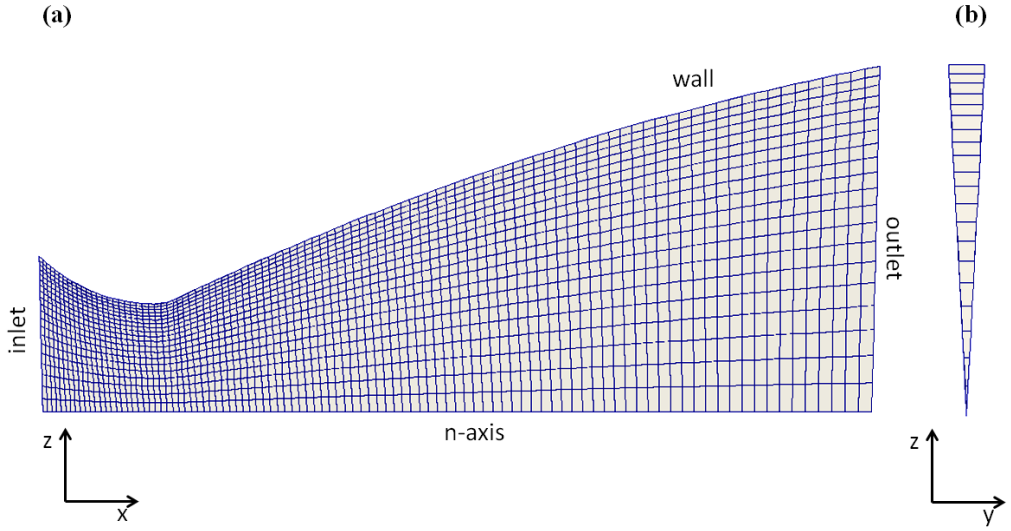

Figure 3. Mesh actually used in the simulations: (a) x-z view and (b) y-z view

3.3 Details of the solution process

I. Initial and boundary conditions

The initial values imposed to the simulation, before achieving steady conditions of the flow in the interior of the nozzle, start with the space inside the nozzle filled with 1,013 MPa (1 atm), 298 K (25^oC) and not moving air. These conditions are also imposed to the outlet surface, in order to establish the situation in the exterior of the nozzle. The density, ρ, can be easily obtained by applying Eq. (10) in all simulation space.

As the nozzle is placed immediately after the catalytic combustion chamber, the conditions in the inlet surface are those of the output of this component. So, the inlet surface provides a not moving fluid with p_0=2,53 MPa, T_0=1461 K, as computed by Miraglia *et al.* (2011). These conditions are kept constant during all the simulation.

II. Solving the equations

The gradients present in Eqs. (5) to (9) are obtained through a standard finite volume discretisation of Gaussian integration which requires the interpolation of values from cell centers to face centers, and the same scheme is used for the divergents. The laplacians are obtained by a Gaussian scheme, along with explicit non-orthogonal correction. If interpolation is need, it is accomplished by a linearization in space of the neighbor's information. For the time discretisation it is used a standard Eulerian scheme.

The algorithm used to perform the integration is the PISO (pressure-implicit split-operator) that implements iterative procedures for solving equations for velocity and pressure, used for transient problems. This algorithm is based on evaluating some initial solutions and then correcting them. Usually, PISO requires more than 1 correction, but typically not more than 4. We specified the number of correctors with a maximum of 2.

III. Visualization / post-processing

The main tool for post-processing and visualization used in this work is the ParaView software. ParaView is an open source, multi-platform data analysis and visualization application, based on client–server architecture to facilitate remote visualization of datasets, and generates level of detail models to maintain interactive frame rates for large datasets. For some other functions and data transformations, some small programs were built with C++, following some of the numerical routines presented by Burian et al (2007).

4 Results

The simulations were run in an Intel i5/3.33 GHz CPU, and the total time was about 2800 s. Initially, the nozzle cavity is initially filled with cold (289 K), one atmosphere, non-moving gas. The inlet boundary was set to the conditions of the combustion chamber, whereas the outlet boundary with the same conditions of the nozzle. The total time of the simulation is 12.5 ms, with data dumps every 0.1 ms interval.

Figure 4 presents the Mach evolution for the simulation during beginning of the simulation and each image represents a 1 ms time step (left-right, top-down). The colors go from deep blue for lower values to red for higher values, and this color scale is used in all figures present in this work. After 7 ms, the Mach number becomes steady and a representation of its final result is presented in Fig. 5. One can see this quantity presents a strong initial variance, followed by an oscillation less strong before entering under steady conditions. This obviously represents a shock due to imposing the hot, high pressure, moving gas to the initial conditions in the interior of the nozzle. The other quantities also present a similar behavior during the first 6-7 ms.

The density is presented in Fig. 6, and the steady state of the overall relative velocity is presented in Fig. 7, in contour levels and vectors. As the magnitude, the components itself in each direction present a strong disturbance in the very beginning of the simulation, and resting in their steady state, following the behavior of the Mach number.

The pressure stabilizes after 5 ms, as one can see from its evolution pictured in Fig. 8 and a representation of its final result is presented in Fig. 9. Figure 10 presents a contour level plot of the steady state of the temperature and Fig. 11 presents the evolution of temperature levels during the first 9 ms.

Figure 12 presents the comparative behaviour of the Mach number (up-left), pressure (up-right), density (down-left) and temperature (down -right) in the axis (r=0) and near the wall. Both plots were taken in a steady state, at the end of the simulation (t=12.5 ms). According to Eq. (1), the theoretical value for the Mach number at the outlet of the nozzle is M_{theo}=3.9. It is observed that the value reached during the simulation to the central (axis) of the nozzle is beyond this value: $M_e|_{r=0}$=4.84. At the same time, the value of the Mach number on the walls, $M_e|_{wall}$, are slightly below 3. One should take into account that the theoretical value is obtained by an expression derived from an exact solution of the Navier-Stokes equations for a quasi-one-dimensional nozzle, and that the simulation presented considers the radial variation of physical quantities. Thus, the theoretical value is in between the two values obtained by the simulation, which is a reasonably good result.

Also, for the pressure, Eq. (2) results in p_{theo}=19.5 kPa, but the simulation resulted in $p_e|_{r=0}$=47.3 kPa and $p_e|_{wall}$=8.5 kPa, what lead us to the same conclusion as above. The same discussion is not valid for density and temperature: the density theoretical value is 21% below the range axis-wall, and the theoretical pressure is 8% above the range axis-wall. Both results must be interpreted keeping in mind that Eqs. (3) and (4) are for a quasi-one-dimensional nozzle. Table 1 presents a compact view of these values.

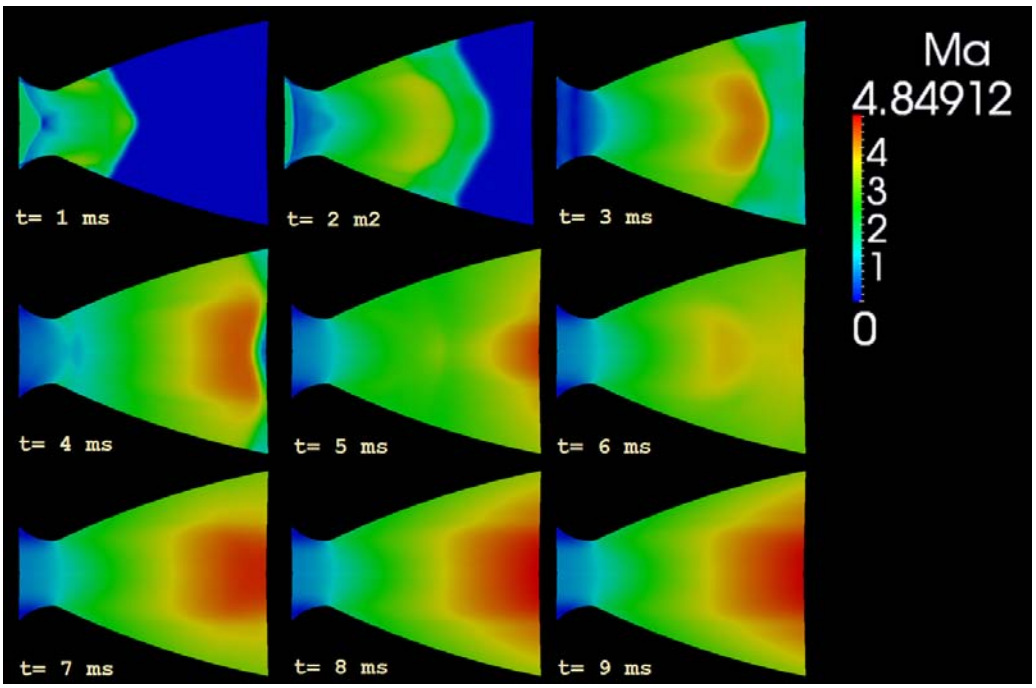

Figure 4. Simulation: evolution of Mach number during the first 9 ms

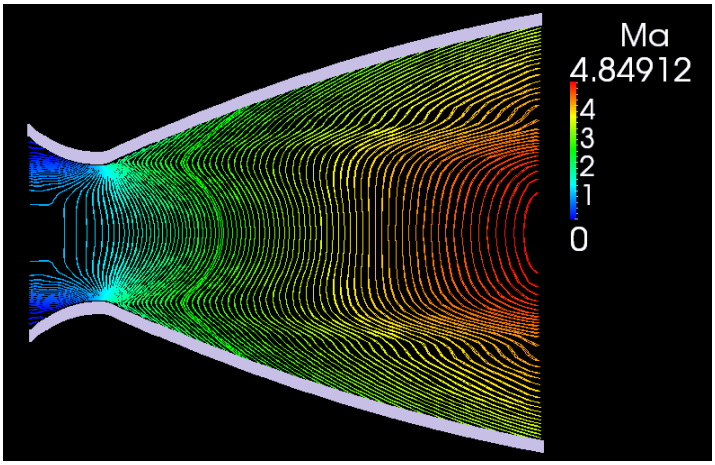

Figure 5. Simulation: steady state of Mach number after 7 ms

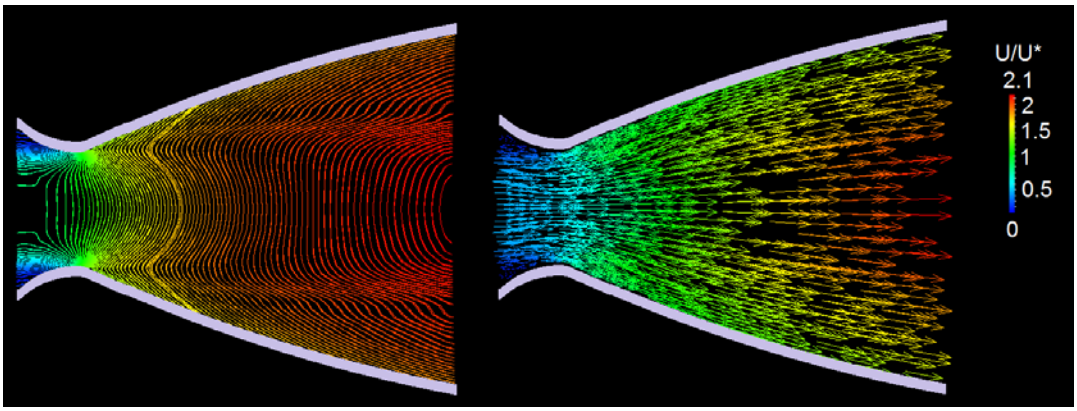

Figure 6. Simulation: steady state of relative velocity after 7 ms. The curves and vectors represent flow velocity relative to its value on the throat

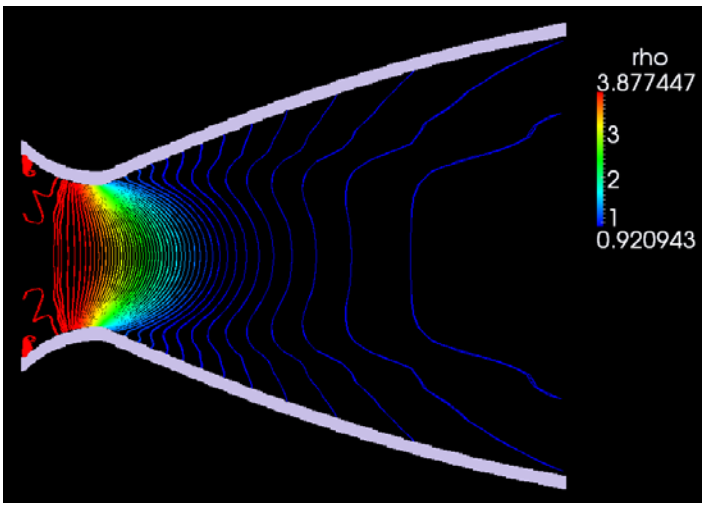

Figure 7. Simulation: steady state of density after 7 ms (units in kg/m^3)

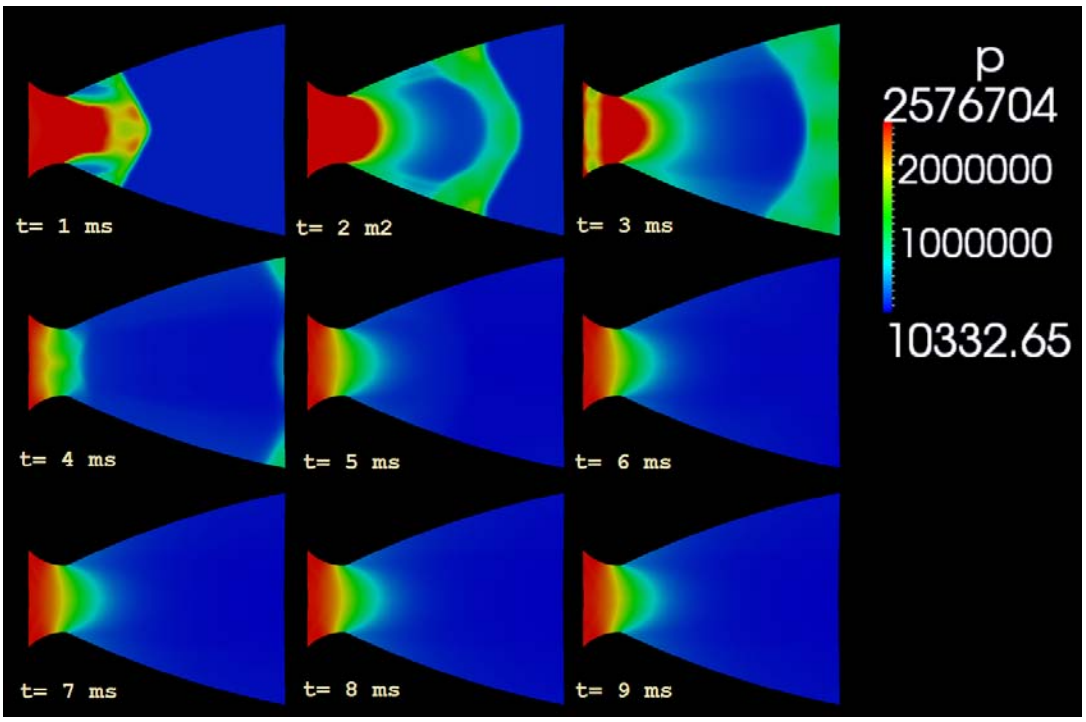

Figure 8. Simulation: evolution of pressure during the first 9 ms (units in Pa)

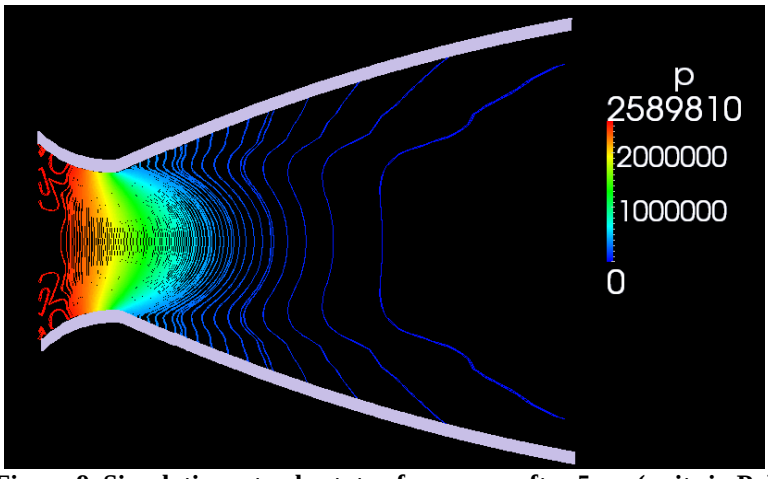

Figure 9. Simulation: steady state of pressure after 5 ms (units in Pa)

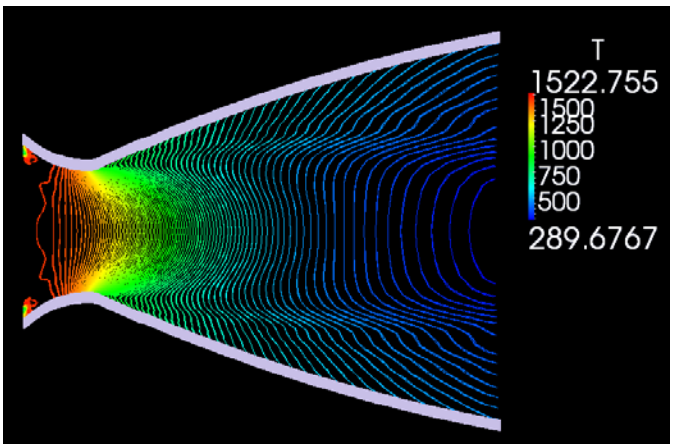

Figure 10. Simulation: steady state of temperature after 6 ms (units in K)

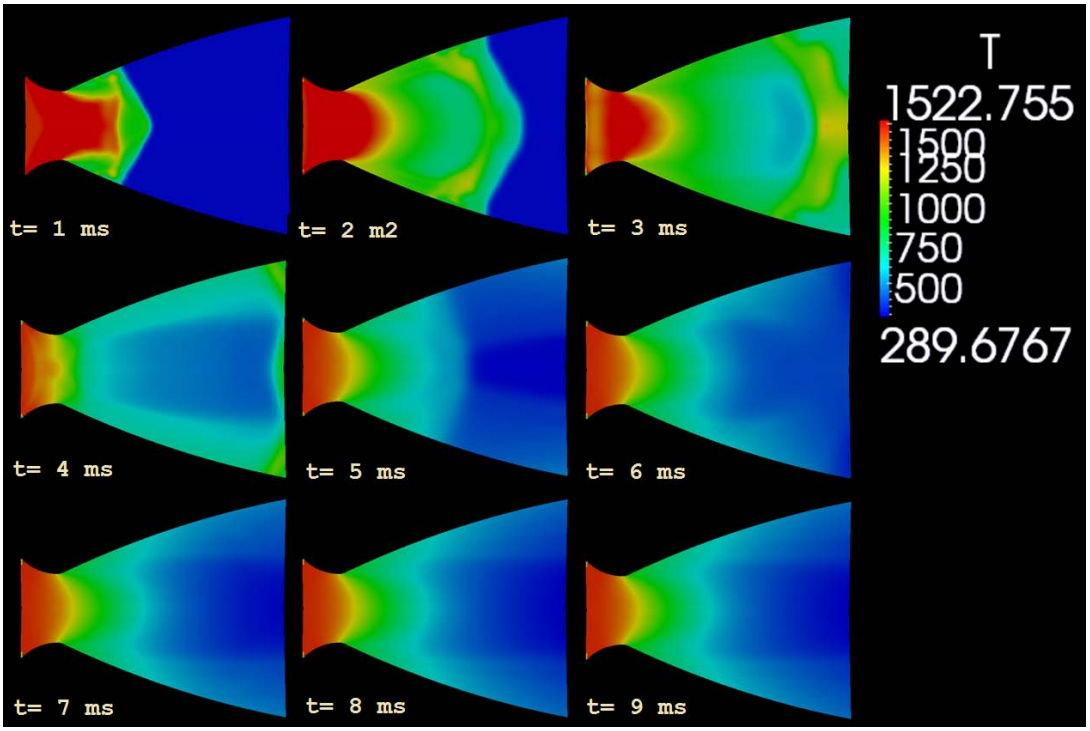

Figure 11. Simulation: evolution of temperature during the first 9 ms (units in K)

For the computation of efficiency and power indexes, namely thrust and specific impulse, one should consider the mass rate and the outlet speed. The results from the catalytic combustion chamber give us $\dot{m} = 1.688$ kg/s, what results in a specific impulse $I_{sp}=V_e\, c/g$ = 168 s and obtained thrust results in 2783 N.

Also in Fig. 12, one can see the properties present discontinuities in their measures along the wall. As far as was possible to assess the discontinuities are due to the low resolution adopted in the construction of the grid calculation. It is intended, with greater computational resources to solve this problem and investigate further this behaviour in future simulations.

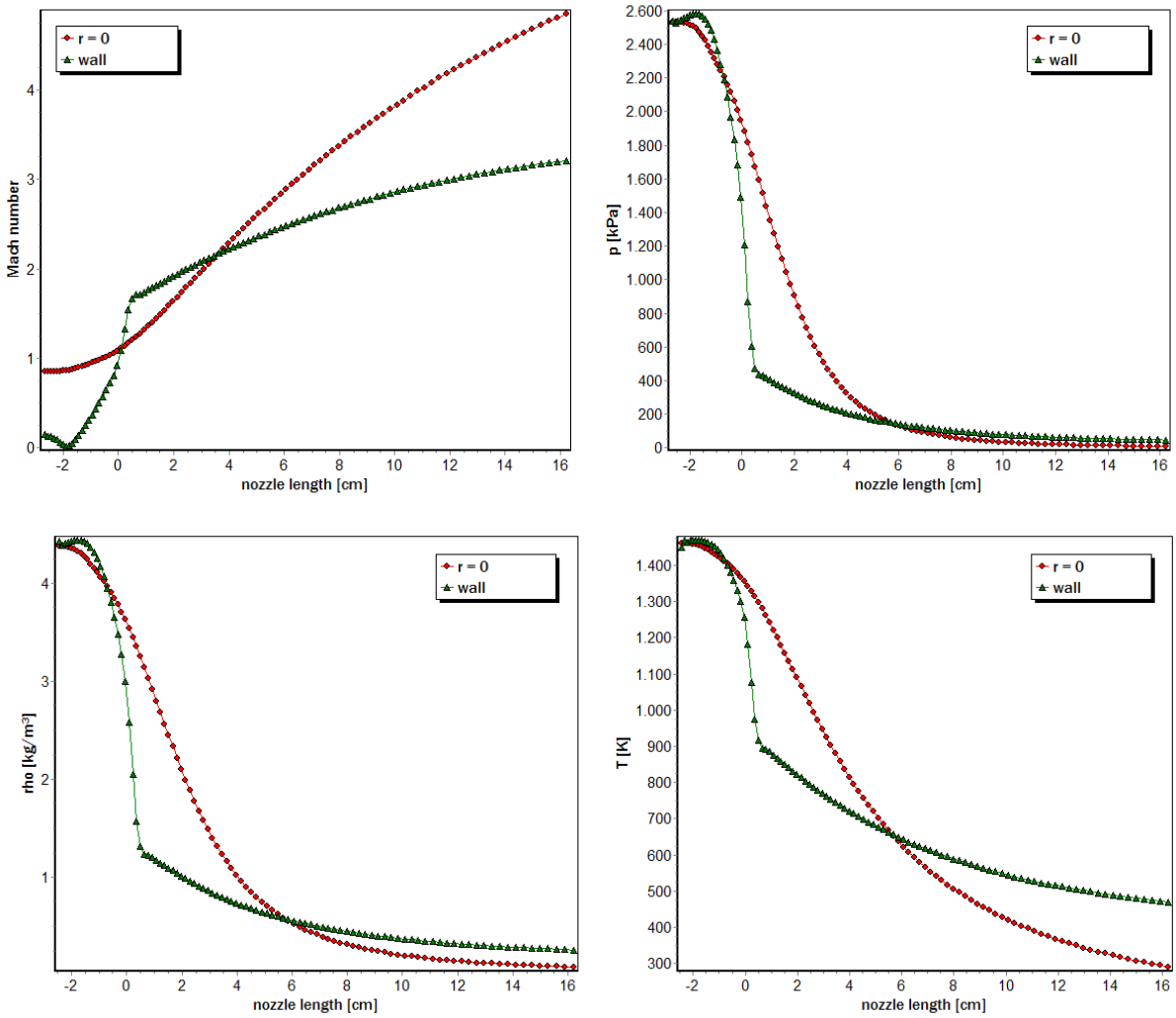

Figure 12. Simulation: steady state of Mach number, pressure, density and temperature at the end of simulations. Both physical quantities are sampled at the central axis and at the nozzle wall

Table 1. Comparison of main quantities obtained by Eqs. (1)-(4) and from the simulation

	Mach number	pressure [kPa]	density [kg/m^3]	temperature [K]
theoretical	3.9	19.5	0.034	486
r=0	4.84	47.3	0.26	470
wall	< 3	8.5	0.08	290

5 Conclusions

The numerical simulations of compressible flow passing through a 3D liquid rocket motor convergent-divergent nozzle with a fixed geometry are carried out. The results are obtained by solving the equations for compressible flow in its conservative form coupled with both the energy equation and the equation of a state over general cylindrical coordinates. In order to solve the governing equations, the numerical method for heat, mass and momentum transfer available in the OpenFOAM package is used. This numerical method is a 3-D finite volume solver based on the PISO algorithm.

From analyzing the results, one can conclude that the catalytic combustion chamber coupled to the described nozzle can produce enough gas expansion to assure the necessary thrust for a small-medium rocket. Still, the numerical results reveal that, the model gave the good results compared with what is expected from this class of nozzle. Some small discrepancies from theoretical results are due to the nature of the exact solutions found for a quasi-one-dimensional interpretation of the problem.

In the next steps of this project are expected simulations of the combustion chamber when will be investigated chemical and thermodynamic details. We also intend to use more computational resources that we had provided more detailed grids both in space and in time.

We intend to continue this preliminary study with more detail about the flow of gas and other elements not yet present in the described simulations. Other nozzle geometries and other relationships between the physical quantities must also be considered, for both laminar and turbulent flow.

Acknowledgments

The authors want to thank the Research Group of Liquid Propellant Rocket of UFABC (http://posmec.ufabc.edu.br/gpmfpl) for supporting this research. C.F.R. thanks the Pro-Rectory of Research of Universidade Federal do ABC for general support.

References

Anderson, J.D., Jr., Computational Fluid Dynamics – The Basics with Applications, McGraw-Hill, 1995.

Balabel, A., Hegab, A.M., Wilson, S., Nasr, M., El-Behery, s. "Numerical Simulation of Turbulent Gas Flow in a Solid Rocket Motor Nozzle",

Bansal, A., Feldick, A., Modest, M.F., "Simulation of Hypersonic Flow and Radiation over a Mars Reentry Vehicle Using OpenFOAM", 50th AIAA Aerospace Sciences Meeting including the New Horizons Forum and Aerospace Exposition: ISBN: 978-1-60086-936-5, 2012.

Böhm, M., "Numerische Strömungsoptimierung: Mathematische Herleitung und exemplarische Umsetzung mit OpenFOAM", VDM Verlag Dr. Müller, ISBN 978-3639328929, 2011.

Bruneau, C. H., Chattot, J. J., Laminie, J., & Guiu-Roux, J., Finite element least square method for solving full steady Euler equations in a plane nozzle, Eighth International Conference on Numerical Methods in Fluid Dynamics, Lecture Notes in Physics, 1982, Volume 170/1982, 161-166, DOI: 10.1007/3-540-11948-5_15.

Burian, R.; Lima, A. C.; Hetem Jr, A. “Cálculo Numérico” LTC - Livros Técnicos e Científicos Editora, 2007.

Cabrit, O. & Artal, L., "Direct Numerical Simulation of Turbulent Multispecies Channel Flow with Wall Ablation", 39th AIAA Thermophysics Conference, 2007.

Cornelisse, J.W., Schoyer, H.F.R., Swakker, K.F., Rocket Propulsion and Space Flight Dynamics, Pitman, 1979.

Davis, R.L., Bulman, M.J., Yam, C., "Numerical Simulation of a Thrust Augmented Rocket Nozzle", Presented at the 42nd AIAA/ASME/SAE/ASEE Joint Propulsion Conference, Sacramento, CA, 9-12 July 2006.

Hagemann, G., Immich, H., Dumnov, G.E., "Advanced Rocket Nozzles", Journal of Propulsion and Power, Vol. 14, No. 5, 1998.

Miraglia, J., Hetem, A., Burian, R., Caetano, C.A.C., Pre-Mixed Liquid Green Propellant for use In Rocket Engines, Proceedings of COBEM 2011 21st Brazilian Congress of Mechanical Engineering, 2011 by ABCM October 24-28, Natal/RN, Brazil.

NASA SP-8120, provided by NASA Astrophysical Data System, 1976.

Pandey, K.M., "CFD Analysis of a Rocket Nozzle with Four Inlets at Mach 2.1", International Journal of Chemical Engineering and Applications, Vol. 1, No. 4, 2010.

Rao, G.V.R., Exhaust Nozzle Contour for Optimum Thrust, Jet Propulsion, Vol. 28, June 1958, pp. 377-382.

Sutton, G.P., & Biblarz, Rocket Propulsion Elements, John Wiley & Sons, 2001.

Torres, M.F.C., Almeida, D.S., Krishna, Y.S.R., Silva, L.A., Shimote, W.K., "Liquid Propulsion and IAE: Vision of the actualities and future perspectives", JATM, v.01 num.1 2009.

Zheng, Q.L., & Sun, L., "The calculation of a compressible flow field by using an open source CFD program", Journal of Harbin Engineering University, v.6, 2011.